

A computational study of magnesium point defects and diffusion in forsterite

Andrew M. Walker^{a,*} Scott M. Woodley^b Ben Slater^{c,d}

Kate Wright^e

^a*Department of Earth Sciences, University of Cambridge, Downing Street,
Cambridge, CB2 3EQ, UK*

^b*Davy Faraday Research Laboratory, 3rd Floor, Kathleen Lonsdale Building,
University College London, Gower Street, London, WC1E 6BT, UK*

^c*Department of Chemistry, 20 Gordon Street, UCL, London, WC1H 0AJ, UK*

^d*Materials Simulation Laboratory, University College London, London, UK*

^e*Nanochemistry Research Institute, Department of Applied Chemistry, Curtin
University of Technology, P.O. Box U1987, Perth 6845, Western Australia*

Abstract

We have studied the formation and migration of point defects within the magnesium sublattice in forsterite using a combination of empirical and quantum mechanical modelling methodologies. Empirical models based on a parameterised force field coupled to a high throughput grid computing infrastructure allow rapid evaluation of a very large number of possible defect configurations. An embedded cluster approach reveals more accurate estimates of defect energetics for the most important defect configurations. Considering all defects in their minimum energy, equilibrium positions, we find that the lowest energy intrinsic defect is the magnesium Frenkel type, where a magnesium atom moves from the M1 site to form a split intersti-

tial defect. This defect has two four coordinated magnesium atoms located outside opposite triangular faces of an otherwise vacant M1 octahedron. The split interstitial defect is more stable than regular interstitials where magnesium is located in either of the two structurally vacant octahedral sites in the hexagonally close packed oxygen lattice. M1 vacancies are also found to form when iron(II) oxidises to iron(III). The energy of the defects away from the equilibrium positions allows the energy barrier to diffusion to be calculated. We have considered the migration of both magnesium vacancies and interstitials and find that vacancies are more mobile. When the contribution from the formation energy of the defects is included we arrive at activation energies for vacancy diffusion that are in agreement with experiment.

Key words: forsterite, olivine, magnesium, defect, diffusion

1 Introduction

2 Although there is a large body of experimental data pertaining to the diffusion
3 of cations in olivine, there has been no determination of the detailed atomic
4 scale mechanism by which cationic defects form and move through the crys-
5 tal lattice. Because of the prevalence of olivine in many mafic and ultramafic
6 igneous rocks such basic information is valuable in the extrapolation of labo-
7 ratory measurements of diffusion for use on a wide variety of geological and
8 geophysical problems. Examples include Fe-Mg exchange in the olivine-spinel
9 mineral pair, which provides an estimate of cooling rates of ultramafic igneous
10 rocks, compositional zoning of olivine crystals growing from a melt, the high

* Corresponding author.

Email address: amw75@cam.ac.uk (Andrew M. Walker).

11 temperature mechanism of electrical conductivity of the upper mantle, as well
12 as the mantle's viscosity and anelasticity.

13 As a relatively simple ternary oxide, cation diffusion in olivine is also of interest
14 as a model material for the materials scientist. Chemically it forms a complete
15 solid solution series with compositions ranging between Mg_2SiO_4 (forsterite,
16 Fo_{100}) and Fe_2SiO_4 (fayalite, Fo_0). The iron-free end member is particularly
17 useful in this regard with no significant opportunity for redox chemistry or
18 exchange between the silicon and magnesium sites. Adding iron provides the
19 possibility for the kind of non-stoichiometry that has been extensively studied
20 in binary oxides such as iron and nickel oxide (Dieckmann, 1998) and these
21 processes have been examined in olivine (Smyth and Stocker, 1975; Stocker
22 and Smyth, 1977; Nakamura and Schmalzried, 1983; Tsai and Dieckmann,
23 1997, 2002).

24 The olivine structure can be viewed as a distorted hexagonally close packed
25 (HCP) array of oxygen ions with half of the octahedral sites and one eighth
26 of the tetrahedral sites occupied by magnesium or iron ions and silicon atoms,
27 respectively. The distortion of the HCP lattice gives the olivine structure or-
28 thorhombic symmetry (space group $Pbnm$) and the unit cell contains four
29 formula units (Figure 1). There are two symmetry distinct octahedral sites:
30 M1, on a centre of symmetry, and M2, on the mirror plane; one distinct tetra-
31 hedral site which lies on the mirror plane and three distinct oxygen sites (O1
32 and O2 on the mirror plane and O3 in a general position). There are also two
33 vacant octahedral sites, I1 on an inversion center and I2 on the mirror plane.
34 Iron and magnesium are generally disordered over the two M sites but at low
35 temperature there is a kinetically hindered tendency to order with iron pref-
36 erentially occupying the M2 octahedra. This effect has been studied using *in*

37 *situ* neutron diffraction and the degree of order can be used as an indicator
38 for cooling rate (e.g. Redfern et al., 1996; Redfern, 1998). The structure can
39 accommodate a range of other cations. For example, calcium is partitioned
40 onto the M2 site to form monticellite (CaMgSiO_4) and manganese, cobalt and
41 nickel olivines can be synthesised. There are also a range of isostructural mate-
42 rials with technological applications. Examples include the olivine phosphates
43 such as LiFePO_4 and LiCoPO_4 which are part of a family of materials with
44 potential applications as cathodes in batteries (Chung et al., 2002; Islam et al.,
45 2005).

46 Because of the technological, geological and basic scientific interest in diffusion
47 in olivine there has been a large number of experimental studies that give the
48 diffusion rate of a number of cations in olivine of various compositions. Exper-
49 imental data includes a series of studies of silicon diffusion (Béjina and Jaoul,
50 1996; Béjina et al., 2003; Dohmen et al., 2002; Houlier et al., 1988; Sockel
51 et al., 1980) and many studies of the diffusion of the M site cations includ-
52 ing magnesium (Bertran-Alvarez et al., 1993; Chakraborty et al., 1994; Sockel
53 and Hallwig, 1977; Sockel et al., 1980), iron (Bertran-Alvarez et al., 1993;
54 Chakraborty, 1997; Jaoul et al., 1995; Nakamura and Schmalzried, 1984) and
55 cobalt (Morioka, 1980). When considering magnesium diffusion, these exper-
56 iments can be separated into two types, those that measure tracer diffusion
57 by diffusing ^{26}Mg into an olivine sample of normal isotopic composition and
58 those that measure the interdiffusion of magnesium and another element be-
59 tween two olivine samples of different chemical compositions. The tracer ex-
60 periments should yield results close to the true self-diffusivity of magnesium
61 in olivine (there is only a small relative mass difference between ^{26}Mg and the
62 normal ^{24}Mg isotope) while interdiffusion experiments yield some average of

63 the diffusivities of the two diffusing elements in olivine with an intermediate
64 composition (see Chakraborty, 1997, for a quantitative discussion).

65 The most complete set of tracer diffusion experiments is that of Chakraborty
66 et al. (1994) who performed experiments on synthetic crystals of forsterite
67 as well as natural samples of San-Carlos olivine ($\text{Fo}_{\approx 90}$) at temperatures be-
68 tween 1000 and 1300 °C under conditions of controlled oxygen fugacity ($p\text{O}_2$).
69 They give activation energies for magnesium diffusion along [001] of $400(\pm 60)$
70 kJmol^{-1} in forsterite and $275(\pm 25)$ kJmol^{-1} in San Carlos olivine and find
71 that cation diffusion is slower along [010] and [100]. However, no activation
72 energies in the slow directions are reported. Magnesium diffusivity in San Car-
73 los olivine was found to vary with $p\text{O}_2$, in fact the diffusivity was found to
74 be directly proportional to $p\text{O}_2^{1/6}$. This result, which is in fair agreement with
75 previous studies (e.g. Nakamura and Schmalzried, 1984, who found diffusivity
76 to be proportional to $p\text{O}_2^{1/5.5}$), suggests that the diffusing species is a mag-
77 nesium vacancy charge balanced by the formation of electron holes or by the
78 oxidation of iron. However, this does not rule out the possibility of diffusion
79 of magnesium interstitial ions formed with a charge neutrality condition in-
80 volving magnesium vacancies and singly charged oxygen vacancies (Stocker
81 and Smyth, 1977). Intriguingly, in the synthetic olivine, the effect of $p\text{O}_2$ is
82 less clear, with different samples giving different results. Two possibilities were
83 put forward, the first invoking a $p\text{O}_2$ dependent change in the mechanism, and
84 the second invoking interstitial Fe(III) ions in the charge neutrality condition.
85 The effect of pressure on magnesium diffusion was also studied and the activa-
86 tion volume was found to be small and positive (about $1 \text{ cm}^3\text{mol}^{-1}$), which is
87 similar to the value derived from interdiffusion experiments (Bertran-Alvarez
88 et al., 1993; Jaoul et al., 1995).

89 Interdiffusion experiments are undertaken by placing two crystals of differ-
90 ing composition together and studying the process by which the two samples
91 approach chemical equilibrium. Two relevant studies are those of Jaoul et al.
92 (1995) and Chakraborty (1997) who studied interdiffusion at 600 – 900 °C and
93 980 – 1300 °C, respectively. Jaoul et al. (1995) performed their experiments
94 at pressures between 0.5 and 9 GPa in piston-cylinder and multi-anvil appa-
95 ratus, extrapolated their data to 0 GPa and Fo₁₀₀ composition, and extracted
96 an activation energy for cation diffusion of 147±58 kJmol⁻¹ along [010]. The
97 experiments at higher temperature (Chakraborty, 1997) yielded an activation
98 energy for cation diffusion along [001] of 226±18 kJmol⁻¹ for olivine of compo-
99 sition Fo₈₆. Recent experiments, using a new thin film based diffusion couple,
100 give activation energies around 200 kJmol⁻¹ for Fe-Mg interdiffusion along all
101 three directions (Dohmen et al., 2007).

102 The effect of dissolved water on cation diffusion in olivine has recently also
103 received attention. Experiments by Wang et al. (2004) and Hier-Majumder
104 et al. (2005) show that magnesium diffusion is at least an order of magnitude
105 more rapid in olivine containing hydrogen than anhydrous olivine of the same
106 composition. However, the activation energy for Fe-Mg interdiffusion between
107 Fo₉₀ and Fo₈₀ along [001] was measured as 220±60 kJmol⁻¹, little different
108 from that measured in anhydrous experiments (see Figure 7 of Hier-Majumder
109 et al., 2005).

110 Although this large body of experimental data is useful for describing the
111 diffusion controlled processes mentioned above, it does not by itself allow the
112 nature of the point defects or the detailed mechanisms by which they move to
113 be determined. In this regard the inherent resolution of atomic scale computer
114 modelling is a particularly useful approach which can yield crucial details of

115 the key processes leading to diffusion. Armed with such an understanding we
116 will be in a much better position to gauge the degree to which experimental
117 data can safely be extrapolated.

118 **2 Methodology**

119 We make use of two complementary methodologies to study defects and diffu-
120 sion on the magnesium sub-lattice of forsterite. First, the formation energies
121 of isolated point defects are studied utilising the Mott-Littleton method with
122 a parameterised potential model (Catlow, 1977b; Sanders et al., 1984; Lewis
123 and Catlow, 1985). These calculations were undertaken employing the GULP
124 code (Gale, 1997; Gale and Rohl, 2003). Further details of the parameters
125 and computational method used can be found in our previous publication on
126 oxygen diffusion in olivine (Walker et al., 2003). These parameters, derived
127 empirically from experimental data for simple binary oxides (supplemented
128 by quantum mechanical data for the oxygen – oxygen interactions), have been
129 successfully used for the modelling of the bulk (e.g. Price et al., 1987; Catlow
130 and Price, 1990) and defect (e.g. Wright et al., 1994; Jaoul et al., 1995; Rich-
131 mond and Brodholt, 2000; Walker et al., 2005) properties of forsterite and of a
132 wide range of other silicates. Selected results are then validated using an em-
133 bedded cluster method. This second method involves modelling the defective
134 crystal using a quantum mechanical (QM) description of the electronic struc-
135 ture of the defect and its immediate surroundings coupled to a parameterised
136 molecular mechanical (MM) model of the crystal further from the defect.

137 For the embedded cluster (QM/MM) calculations we made use of the GUESS
138 code (Sushko et al., 2000b,a) following the recipe described in Braithwaite

139 et al. (2002, 2003), Walker et al. (2006) and Berry et al. (2007). Briefly, the
140 simulation consists of a small inner QM cluster containing 43 ions when no
141 defects are present, which is embedded within a MM nanocluster of radius
142 30 Å. In these calculations the inner QM cluster is described using a either
143 Hartree-Fock, Density Functional, or a hybrid B3LYP Hamiltonian using the
144 Gaussian98 package (Frisch et al., 1998). The MM nanocluster is modelled
145 using a potential model fitted to be consistent with the QM charges and all
146 atoms (QM and MM) within 12 Å of the center of the model are allowed to
147 relax to an energy minimum.

148 The methodology for studying magnesium diffusion by the vacancy mechanism
149 was identical to that described for oxygen diffusion (Walker et al., 2003) – we
150 define possible paths that a magnesium ion could take between adjacent M
151 sites and perform a series of constrained geometry optimizations with the ion
152 held fixed on this path (between two magnesium vacancies). These calculations
153 are then used to determine a starting geometry for a transition state search
154 algorithm based on the Rational Function Optimization (RFO) procedure
155 described by Banerjee et al. (1985) and implemented in GULP. (A starting
156 point close to the transition state is needed in order to avoid the optimizer
157 locating other, less relevant, transition states.) The energy of the defects away
158 from their equilibrium positions is evaluated using the Mott-Littleton method
159 and we break diffusion down into a series of “hops” between adjacent sites.
160 Each hop is associated with a migration energy barrier. By making a series
161 of hops, the diffusing ion may cross the unit cell. Under the assumption that
162 consecutive hops are uncorrelated, the maximum migration energy required to
163 achieve movement in a particular direction is the activation energy for diffusion
164 in that direction. In order to go beyond the activation energy and extract

165 the diffusion coefficient would require dynamical information that could be
166 obtained from lattice dynamics coupled with Vineyard theory (e.g. Vočadlo
167 et al., 2006). But for a low symmetry structure such as forsterite, further
168 kinetic Monte Carlo analysis of the results would be required.

169 Because of the apparent complexity of the potential energy surface discovered
170 in the search for the geometry of magnesium interstitial defects described
171 in section 3.2, a different approach was used for interstitial diffusion. The
172 general approach is similar; the potential energy surface is first mapped to
173 locate approximate saddle points and then an RFO transition state search
174 is performed, but the method of locating the approximate saddle point is
175 different. Rather than predetermining individual steps for diffusion, a large
176 segment of the potential energy surface corresponding to moving the intersti-
177 tial magnesium ion and relaxing the rest of the structure was evaluated. This
178 required 2000 separate Mott-Littleton calculations which were completed in
179 parallel using emerging grid computing technology. In particular we make use
180 of the large Condor pool at University College London (Wilson et al., 2004),
181 which harnesses hundreds of teaching computers to provide a significant high
182 throughput computing resource. Transition states on this surface are then lo-
183 cated using an iterative basin filling methodology. The approach, described
184 in more detail by Woodley and Walker (2007), involves the location of the
185 global minimum followed by incrementally increasing an excess energy and
186 determining for the volume a diffusing ion with this energy can sample. When
187 this accessible volume first includes a neighboring periodic image of the global
188 minimum, a transition state and energy barrier is located.

189 **3 Results**

190 *3.1 Magnesium vacancies*

191 Using the Mott-Littleton method, the formation energy (energy associated
192 with removing a single ion from the lattice to an isolated state) of a vacancy
193 on the M1 site is calculated as 24.5 eV while the formation energy of an
194 M2 vacancy is 26.4 eV. This means that essentially all magnesium vacancies
195 should form on the M1 site and the energy difference is in good agreement
196 with previous calculations using interatomic potentials and periodic Density
197 Functional Theory (Brodholt, 1997).

198 The embedded cluster calculations, which are limited to calculations of the
199 M1 vacancy, are in good agreement with the Mott-Littleton results, with cal-
200 culated defect energy approximately 0.5 eV lower than the Hartree-Fock (HF)
201 result. This agreement is hardly surprising given that magnesium is an ionic
202 species in forsterite. Mulliken population analysis of the electron density gives
203 charges in the region of +2 electronic units, and the parameterised potential
204 is a good description of a formally charged, spherical closed shell ion.

205 The embedded cluster calculations show few basis set truncation effects (Ta-
206 ble 1); explicit relaxation with a 6-31+G* or 6-311+G* basis set (Foresman
207 and Frisch, 1996, give an outline of the meaning of these codes) alters the
208 calculated energy by less than 0.1 eV. Calculations using the HF approxima-
209 tion give the lowest defect energy while DFT with the PW91 functional gives
210 the largest defect energy (almost 1 eV higher in energy than the HF result)
211 suggesting that correlation effects tend to increase the binding of Mg to the

212 forsterite lattice. As expected, the B3LYP hybrid functional yields intermedi-
213 ate energies.

214 3.2 *Interstitial defects*

215 In practical terms, while vacancies are created by simply removing the relevant
216 ion from the simulation cell more effort is required to establish the structure of
217 interstitials. In the case of interstitial magnesium, location of energy minima
218 was far from straightforward. Initial calculations with interstitial magnesium
219 ions in either of the two vacant octahedral sites resulted in very large ionic
220 displacements on relaxation and final defect energies that were very sensitive
221 to the initial geometry. This is an indication of a failure of the geometry op-
222 timisation procedure, probably due to a starting configuration away from an
223 energy minimum on a complex energy hypersurface. In order to locate the
224 minimum energy configuration for a magnesium interstitial, a large number
225 of starting geometries were created by placing interstitial magnesium ions on
226 a regular 0.5 Å grid across the symmetry irreducible portion of the unit cell
227 and performing an optimisation of all atomic coordinates (including the lo-
228 cation of the interstitial) using the UCL Condor pool. Following removal of
229 unphysical structures, where the Coulombic attraction between oxygen ions
230 and magnesium ions had overcome the short range repulsion leading to very
231 large negative energies, the lowest energy structures were examined. The low
232 energy configurations were all split interstitials, where the interstitial ion and
233 a displaced lattice magnesium ion were located close to opposite faces of an
234 M1 or M2 octahedron. Embedded cluster calculations show that the split
235 interstitial is substantially more stable (4.4 eV lower in energy) than an oc-

236 tetrahedrally co-ordinated magnesium interstitial on the I1 site. The reason for
237 the preference for tetrahedrally co-ordinated magnesium split interstitial de-
238 fects over octahedrally coordinated interstitial defects on the I1 or I2 site is
239 not immediately obvious on structural grounds. However, at least part of the
240 destabilization of octahedral interstitials is due to electrostatic interactions
241 between the interstitial and the rest of the crystal, which is best described
242 by the electrostatic potential on the site. We find that this is positive which
243 explains the low stability of a positively charged magnesium ion on the site
244 and accounts for the stability of negatively charged, octahedrally coordinated
245 oxygen interstitials (Walker et al., 2003).

246 The lowest energy site was chosen for further investigation and Mott-Littleton
247 and embedded cluster calculations were set up with the structure (with two
248 interstitial ions and a vacancy) as input. The Mott-Littleton approach gave
249 a formation energy of -17.75 eV and the embedded cluster calculations give
250 similar values, reported in Table 2. Details of the structure derived from the
251 embedded cluster calculation is shown in Figure 2. The two magnesium ions
252 form a split interstitial across the M1 site orientated in the [010] direction
253 with each magnesium ion in distorted tetrahedral co-ordination, in agreement
254 with the structure from the Mott-Littleton calculations. The Mg – O bond
255 distances are similar to those found in crystals with structural magnesium
256 tetrahedrally co-ordinated by oxygen. For example in a recently synthesised
257 bismuth magnesium vanadate (Uma and Sleight, 2002) tetrahedral Mg – O
258 bonds are ~ 1.95 Å long, and in the tetragonal Mg_2TiO_4 spinel bond lengths
259 are 1.995 and 1.981 Å (Millard et al., 1995). In the split interstitial defect the
260 bonds are 1.89, 2.02, 1.96 and 1.86 Å long for the Mg – O3a, Mg – O1, Mg –
261 O3b and Mg – O2 bonds, respectively.

262 The energies of the magnesium split interstitial defect calculated using the
263 QM/MM method and shown in Table 2 are in excellent agreement with the
264 Mott-Littleton methodology. The HF approximation predicts defect energies
265 almost 1 eV higher than DFT, while B3LYP and GGA DFT agree to within
266 better than 0.05%. The Mott-Littleton results fall between those of HF and
267 DFT. Convergence with basis set size is not as good as in the case of the
268 magnesium vacancy (perhaps due to the partial occupation of d-orbitals not
269 represented in the smaller basis sets), but in any case the change in energy
270 from the 6-31+G**//6-31-G to 6-311+G**//6-311+G* is only about 0.1 eV.

271 3.3 Diffusion

272 In order to study vacancy diffusion we first defined paths between all adjacent
273 M sites in the olivine structure. Figure 3 shows the five inequivalent routes
274 between magnesium vacancies that we consider may be involved in magnesium
275 vacancy diffusion. Hop A is between two M1 sites along [100] through the
276 vacant octahedral I1 interstitial position while hop B is between two M2 sites
277 along [100] through the vacant octahedral I2 position. Hop C is between two
278 M2 positions with displacement mostly within an (001) plane. Hops D and E
279 are from M1 sites to M2 sites with D mostly within the (100) plane and E
280 with significant components in all three crystallographic directions. Hops D'
281 and E' are the reverse hops from M2 sites to M1 sites. Hop F is between two
282 M1 sites along [001].

283 Migration energies for each of these hops is given in Table 3, in addition the
284 transition states for interstitial diffusion are also shown. There are several
285 points to note. First, the large barriers to diffusion through the vacant I1 and

286 I2 octahedra (hops A and B) is somewhat surprising given the expectation
287 that magnesium “prefers” an octahedral environment, and especially given
288 that the transition state is found to be in close to the centre of the octahedron.
289 It seems likely that this is a Coulombic effect that is also responsible for the
290 lack of stable octahedrally co-ordinated magnesium interstitials (as described
291 in section 3.2, above). Vacancy diffusion along [001] is predicted to be via
292 hop F with the low activation energy of 0.72 eV and diffusion along [100] and
293 [010] is predicted to be via hops D and C with a extrinsic activation energy
294 controlled by hop D with a value of 1.98 eV. This is a lower barrier then that
295 found for interstitial diffusion. Therefore interstitial diffusion is not favoured
296 over vacancy diffusion in any direction. The energy barrier for hop F has
297 also been calculated by B ejina et al. (2008) using periodic density functional
298 theory. These calculations give an upper bound on the barrier hight of 0.84
299 eV, showing that at least this energy barrier is well modeled by the force field
300 model.

301 4 Discussion

302 The defect formation energies presented in the preceding sections represent
303 the internal energy contribution needed to remove an ion from the lattice to
304 the gas phase, and to bring an ion from the gas phase, to form vacancies or
305 interstitials, respectively. Thus this energy does not represent any real process.
306 However, before considering more realistic defect reactions, we first address the
307 accuracy of the calculations. As far as we are aware, there is no experimental
308 data that directly constrains defect thermodynamics although some studies
309 give important insights. Instead of considering agreement with experiment,

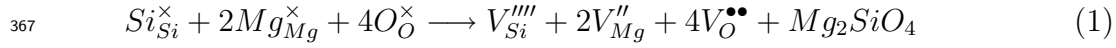
310 the consistency of the present results with previous computational studies will
311 be considered. Results from the potential model presented in Table 4 (which
312 includes a summary of the results of this paper) are in excellent agreement with
313 previous work using the same potential model, this includes work that utilised
314 the super-cell approach (Richmond and Brodholt, 2000) as well as the Mott-
315 Littleton method used here (Wright and Catlow, 1994; Jaoul et al., 1995). This
316 is hardly surprising – indeed disagreement would have suggested errors in one
317 or more of the codes used to perform the calculations. An additional test of
318 the accuracy of the potentials based defect energetics is by comparison with
319 the results of electronic structure calculations. In general, as was pointed out
320 in the results sections, good agreement with such calculations is observed. In
321 particular the defect formation energies calculated using the embedded cluster
322 methodology by Braithwaite et al. (2002, 2003), as well as the additional
323 results presented here, are in general agreement with the calculated atomistic
324 values. Discrepancies between results obtained using the potential model and
325 electronic structure methods, and between results from the embedded cluster
326 method and periodic DFT calculations, have been noted by Braithwaite et al.
327 (2003) and Brodholt (1997). The largest error is associated with the formation
328 of a vacancy on the silicon site. The first reason for this error is likely to be that
329 the potential model is unable to describe the resultant five co-ordinate silicate
330 species. A second consideration is that the charge on the silicon vacancy is
331 the largest considered – resulting in the largest correction terms for the long-
332 range polarization and the largest electronic polarisation, especially of the
333 oxygen ions. It is possible that the basis set is not sufficient for modelling this
334 polarisation. Although some of this difference can be attributed to the small
335 size of the super-cell it is likely that an additional factor is caused by the way
336 electronic polarisation around the defect is treated in the atomistic and density

337 functional calculations. In the DFT study it is likely that the polarisation
338 is under-estimated around the highly charged silicon vacancy because of an
339 inadequate plane wave basis that was only converged with respect to bulk
340 olivine (this would destabilise the defect, as it would have a larger effective
341 charge). On the other hand, the simple shell model used in our potential based
342 calculations could easily overestimate the polarization of oxygen close to the
343 defects, which would tend to make the defects too stable.

344 Some additional energies are needed in order to consider the defect reactions,
345 these include the enthalpy of formation of a number of minerals that will be
346 the source or sink of the ions from the defect and a number of other standard
347 energies. These are given in Table 4, with formation energies calculated using
348 the same interatomic potential model used to calculate the defect structures
349 and energies.

350 Crystals at thermodynamic equilibrium contain a number of point defects be-
351 cause the entropy gained in forming the defects outweighs the energetic penalty
352 of forming the defect. For simple uncharged defects the defect concentration at
353 a given temperature can be calculated in a straightforward manner. First the
354 the free energy change in terms of the enthalpy of the formation of the point
355 defect and the configurational entropy gained as a function of defect concen-
356 tration is explicitly expressed. Then this expression is differentiated to find
357 the minimum free energy, giving the equilibrium defect concentration. Such a
358 procedure is much more complex in multi-component ionic systems because
359 there are a range of possible defect types. In principle one should minimise
360 the free energy numerically, taking into account the enthalpic and entropic
361 contribution from all possible defect species under an imposed condition of
362 charge neutrality (Ashcroft and Mermin, 1976). The first stage requires the

363 calculation of possible reactions resulting in the formation of intrinsic defects,
 364 which is undertaken here. Using the results of the Mott-Littleton calculations
 365 gives the energy of a full Schottky defect where a full formula unit of forsterite
 366 vacancies is formed and the ions are moved to the surface as:



$$368 \quad E = E(V_{Si}^{''''}) + 2(2V_{Mg1}^{''}) + 4E(V_{O3}^{\bullet\bullet}) + U_{Mg_2SiO_4} = 35.44eV$$

369 or 5.06 eV per defect. This can be compared with a value of 30.25eV given
 370 by GGA calculated using a super-cell containing 56 atoms (Brodholt, 1997).
 371 Additional calculations using the same potentials and a fully converged super
 372 cell gives better agreement with the Mott-Littleton calculations (36.4 eV).
 373 Decreasing the size of the super cell will tend to reduce this value explaining
 374 the discrepancy.

375 The second major type of intrinsic defect is the Frenkel defect where a vacancy
 376 is charge balanced by an interstitial of its own type. In principle, Frenkel
 377 defects can form on any of the three sublattices. The oxygen Frenkel:



$$379 \quad E = E(O_{I2}^{''}) + E(V_{O3}^{\bullet\bullet}) = 8.43eV$$

380 gives a defect energy of 4.22 eV per defect formed, while the magnesium
 381 Frenkel:



$$383 \quad E = E(Mg_{I-split}^{\bullet\bullet}) + E(V_{Mg1}^{''}) = 6.73eV$$

384 yields an energy of 3.37 eV per defect, and the silicon Frenkel defect gives:



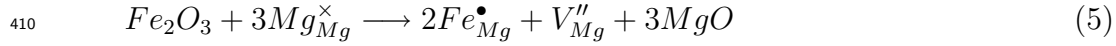
$$386 \quad E = E(Si_I^{\bullet\bullet\bullet\bullet}) + E(V_{Si}^{\prime\prime\prime\prime}) = 24.21 eV$$

387 or 12.10 eV per defect. Clearly the Mg Frenkel defect will be the predominant
388 intrinsic defect, in agreement with the suggestion of Smyth and Stocker (1975),
389 but this does not rule out the possibility of other intrinsic defects (indeed they
390 are required to minimise the free energy).

391 The migration energies presented in section 3.3 equate to activation energies
392 for extrinsic diffusion (in the classical sense), and are within error of the exper-
393 imental results of Jaoul et al. (1995), after their pO_2 correction. For intrinsic
394 diffusion (pure Mg_2SiO_4 with thermally created point defects) an appropriate
395 defect formation energy must be added. Our results suggest that the appro-
396 priate defect reaction is the magnesium Frenkel defect, and 3.37 eV should
397 be added to the predicted migration energies to yield the intrinsic activation
398 energy. This results in activation energies of 5.35 eV (513 kJmol^{-1}) along [100]
399 and [010] and 4.09 eV (393 kJmol^{-1}) along [001], which is within the stated
400 error of the results of Chakraborty et al. (1994) for higher temperatures where
401 intrinsic diffusion may be expected. The sense of the anisotropy in activation
402 energy is also correctly described although no experimental results for the
403 activation energy along the slow directions have been presented.

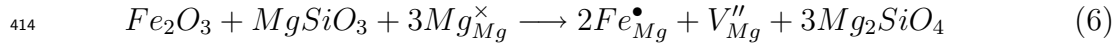
404 For iron bearing olivine Chakraborty et al. (1994) extracted significantly lower
405 activation energies, presumably because the magnesium vacancies are formed
406 at lower energetic cost. One way to form magnesium vacancies is to charge
407 balance their formation with the oxidation of iron, or by the incorporation of

408 ferric iron. Using energies of iron defects calculated by Walker et al. (2003),
 409 this process can be represented by the reaction:



$$411 \quad E = 2E(Fe_{Mg}^{\bullet}) + E(V_{Mg}'') + 3U(MgO) - U(Fe_2O_3) = 4.47eV$$

412 In the mantle, it would be more realistic for excess MgO to react with pyroxene
 413 to form olivine:



$$415 \quad E = 2E(Fe_{Mg}^{\bullet}) + E(V_{Mg}'') + 3U(Mg_2SiO_4) - U(Fe_2O_3) - 3U(MgSiO_3) = 3.81eV$$

416 Adding one third of these energies (1.49 or 1.27 eV) to the [001] migration
 417 energy yields a predicted activation energy of 2.21 or 1.99 eV (213 or 192
 418 kJmol⁻¹), respectively. This is a little lower than the 275±25 kJmol⁻¹ mea-
 419 sured for tracer diffusion by Chakraborty et al. (1994).

420 5 Conclusions

421 The calculations reported here point to a number of interesting results. First,
 422 in pure forsterite the majority intrinsic defect species is predicted to be the
 423 magnesium Frenkel defect. This does not rule out the possibility of defects on
 424 the silicon or oxygen lattices – indeed these are required at equilibrium – but
 425 does indicate that electrical conductivity, for example, may be controlled by
 426 these defects. There has been at least one theoretical study of the intrinsic
 427 conductivity of forsterite (Morin et al., 1977, 1979), this analysed the likely
 428 introduction of bands in the band gap in forsterite on the basis of a comparison

429 with MgO and quartz. The conclusion was that intrinsic conductivity can be
430 explained by postulated magnesium interstitials on the unoccupied octahedral
431 site. The results given above suggest that such defects do not exist and instead
432 the split interstitial defect should predominate; the need for a re-evaluation
433 of intrinsic conductivity data is therefore suggested. In any case, electrical
434 conductivity of olivine under mantle conditions is likely to be controlled by
435 hydrogen diffusion, which is one reason for the major interest in hydrogen
436 speciation in upper mantle rocks. In addition to the energies of defects in
437 forsterite, the defect states in the surrounding minerals should be considered
438 along with the temperature and pressure. Such an analysis is beyond the scope
439 of the current work, but the importance of the oxidation and reduction of iron
440 in the lattice is established.

441 A further interesting observation is that oxygen ions are able to form intersti-
442 tial defects in the vacant octahedral sites in the olivine structure but, perhaps
443 surprisingly, magnesium ions are unstable in this environment. The reason
444 for this seems to be at least partially due to the electrostatic interactions be-
445 tween the defect and the rest of the crystal, best described by the electrostatic
446 potential on the site. This is positive, so negatively charged oxygen ions are
447 stabilised by the electrostatic potential while positively charged magnesium
448 ions on the site are penalised.

449 The results for magnesium diffusion are in agreement with previous compu-
450 tational studies Jaoul et al. (1995) and agree to a remarkable degree with the
451 experimental data. The data of Jaoul et al. (1995) and Chakraborty et al.
452 (1994) for magnesium diffusion in San Carlos olivine can be interpreted as
453 the diffusion of magnesium vacancies charge balanced by iron(III) (with the
454 iron oxidation either corrected to extract “true” extrinsic activation energies

455 or included in the calculation of the activation energy). The higher activation
456 energy measured by Chakraborty et al. (1994) in synthetic forsterite seems
457 to indicate that true intrinsic diffusion, with magnesium Frenkel defects pro-
458 viding the source of vacancies, was measured in that case. The diffusion of
459 magnesium interstitials is not favoured over vacancy diffusion, a conclusion
460 reinforced by the many measurements of positive pO_2 dependence of magne-
461 sium diffusion in olivine.

462 **6 Acknowledgments**

463 A.M.W. acknowledges the receipt of a studentship from the Engineering and
464 Physical Sciences Research Council and K.W. thanks the Royal Society for a
465 University Research Fellowship.

466 **References**

- 467 Ashcroft, N. W., Mermin, N. D., 1976. Solid State Physics. Saunders College,
468 Orlando.
- 469 Banerjee, A., Adams, N., Simons, J., Shepard, R., 1985. Search for stationary
470 points on surfaces. *Journal of Physical Chemistry* 89 (1), 52 – 57.
- 471 Bějina, F., Jaoul, O., 1996. Silicon self diffusion in quartz and diopside mea-
472 sured by nuclear micro-analysis methods. *Physics of the Earth and Plane-
473 tary Interiors* 97, 145 – 162.
- 474 Bějina, F., Jaoul, O., Liebermann, R. C., 2003. Diffusion in minerals at high
475 pressure: a review. *Physics of the Earth and Planetary Interiors* 139, 3 – 20.
- 476 Bějina, F., Blanchard, M., Wright, K., Price, G. D., 2008. A computer simu-

477 lation study of the effect of pressure on Mg diffusion in forsterite. *Physics*
478 *of the Earth and Planetary Interiors*, this issue.

479 Berry, A. J., Walker, A. M., Hermann, J., O'Neill, H. S., Foran, G. J., Gale,
480 J. D., 2007. Titanium substitution mechanisms in forsterite. *Chemical Ge-*
481 *ology* 242, 176 – 186.

482 Bertran-Alvarez, Y., Jaoul, O., Liebermann, R. C., 1993. Fe-Mg interdiffusion
483 in single crystal olivine at very high pressure and controlled oxygen fugacity:
484 technological advances and initial data at 7 GPa. *Physics of the Earth and*
485 *Planetary Interiors* 70, 102 – 118.

486 Braithwaite, J. S., Sushko, P. V., Wright, K., Catlow, C. R. A., 2002. Hydrogen
487 defects in forsterite: A test case for the embedded cluster method. *Journal*
488 *of Chemical Physics* 116 (6), 2628–2635.

489 Braithwaite, J. S., Wright, K., Catlow, C. R. A., 2003. A theoretical study of
490 the energetics and IR frequencies of hydroxyl defects in forsterite. *Journal*
491 *of Geophysical Research Solid Earth* 108 (B6), 2284, article number 2284.

492 Brodholt, J. P., 1997. Ab initio calculations on point defects in forsterite
493 (Mg_2SiO_4) and implications for diffusion and creep. *American Mineralogist*
494 82, 1049 – 1053.

495 Catlow, C. R. A., 1977b. Point defect and electronic properties of uranium
496 dioxide. *Proceedings of the Royal Society of London A.* 353, 533 – 561.

497 Catlow, C. R. A., Price, G. D., 1990. Computer modelling of solid-state inor-
498 ganic materials. *Nature* 347, 243–347.

499 Chakraborty, S., 1997. Rates and mechanisms of Fe-Mg interdiffusion in
500 olivine at 980°C - 1300°C. *Journal of Geophysical Research* 120 (B6), 12317–
501 12331.

502 Chakraborty, S., Farver, J. R., Yund, R. A., Rubie, D. C., 1994. Mg tracer
503 diffusion in synthetic forsterite and San Carlos olivine as a function of P, T

504 and fO₂. *Physics and Chemistry of Minerals* 21, 489 – 500.

505 Chung, S. Y., Bloking, J. T., Chiang, Y. M., 2002. Electronically conductive
506 phospho-olivines as lithium storage electrodes. *Nature Materials* 1 (2), 123–
507 128.

508 Dieckmann, R., 1998. Point defects and transport in non-stoichiometric oxides:
509 solved and unsolved problems. *Journal of Physics and Chemistry of Solids*
510 59 (4), 507–525.

511 Dohmen, R., Chakraborty, S., Becker, H.-W., 2002. Si and O diffusion in
512 olivine and implications for characterizing plastic flow in the mantle. *Geo-
513 physical Research Letters* 29 (21), 2030.

514 Dohmen, R., Becker, H.-W., Chakraborty, S., 2007. Fe-Mg diffusion in olivine
515 I: experimental determination between 700 and 1,200°C as a function of
516 composition, crystal orientation and oxygen fugacity. *Physics and Chemistry
517 of Minerals* 34, 389-407.

518 Foresman and Frisch (1996) *Exploring Chemistry with Electronic Structure
519 Methods*. 302 pp. Gaussian Inc. Pittsburgh.

520 Frisch, M. J., Trucks, G. W., Schlegel, H. B., Scuseria, G. E., Robb, M. A.,
521 Cheeseman, J. R., Zakrzewski, V. G., J. A. Montgomery, J., Stratmann,
522 R. E., Burant, J. C., Dapprich, S., Millam, J. M., Daniels, A. D., Kudin,
523 K. N., Strain, M. C., Farkas, O., Tomasi, J., Barone, V., Cossi, M., Cammi,
524 R., Mennucci, B., Pomelli, C., Adamo, C., Clifford, S., Ochterski, J., Peters-
525 son, G. A., Ayala, P. Y., Cui, Q., Morokuma, K., Malick, D. K., Rabuck,
526 A. D., Raghavachari, K., Foresman, J. B., Cioslowski, J., Ortiz, J. V.,
527 Baboul, A. G., Stefanov, B. B., Liu, G., Liashenko, A., Piskorz, P., Ko-
528 maromi, I., Gomperts, R., Martin, R. L., Fox, D. J., Keith, T., Al-Laham,
529 M. A., Peng, C. Y., Nanayakkara, A., Gonzalez, C., Challacombe, M., Gill,
530 P. M. W., Johnson, B. G., Chen, W., Wong, M. W., Andres, J. L., Head-

531 Gordon, M., Replogle, E. S., Pople, J. A., 1998. Gaussian 98 (revision a.7).
532 Gale, J. D., 1997. GULP: A computer program for the symmetry-adapted
533 simulation of solids. *Journal of the Chemical Society, Faraday Transactions*
534 *93* (4), 629 – 637.

535 Gale, J. D., Rohl, A. L., 2003. The general utility lattice program (GULP).
536 *Molecular Simulation* *29* (5), 291 – 341.

537 Hier-Majumder, S., Anderson, I. M., Kohlstedt, D. L., 2005. Influence of pro-
538 tons on Fe-Mg interdiffusion in olivine. *Journal of Geophysical Research*
539 *110*, B02202.

540 Houlier, B., Jaoul, O., Abel, F., Liebermann, R. C., 1988. Oxygen and silicon
541 self-diffusion in natural olivine. *Physics of the Earth and Planetary Interiors*
542 *50*, 240 – 250.

543 Islam, M. S., Driscoll, D. J., Fisher, C. A. J., Slater, P. R., 2005. Atomic-
544 scale investigation of defects, dopants and lithium transport in the LiFePO₄
545 olivine-type battery material. *Chemistry of Materials* *17*, 5085 – 5092.

546 Jaoul, O., Bertran-Alvarez, Y., Liebermann, R. C., Price, G. D., 1995. Fe-Mg
547 interdiffusion in olivine up to 9 GPa at T = 600-900°C; experimental data
548 and comparison with defect calculations. *Physics of the Earth and Planetary*
549 *Interiors* *89*, 199 – 218.

550 Lewis, G. V., Catlow, C. R. A., 1985. Potential models for ionic oxides. *Journal*
551 *of Physics C: Solid State Physics* *18*, 1149 – 1161.

552 Millard, R. L., Peterson, R. C., Hunter, B. K., 1995. Study of the cubic to
553 tetragonal transition in Mg₂TiO₄ and Zn₂TiO₄ spinells by ¹⁷O MAS NMR
554 and Rietveld refinement of X-ray diffraction data. *American Mineralogist*
555 *80*, 885 – 896.

556 Morin, F. J., Oliver, J. R., Housley, R. M., 1977. Electrical properties of

557 forsterite, Mg_2SiO_4 . *Physical Review B* 16 (10), 4434 – 4445.

558 Morin, F. J., Oliver, J. R., Housley, R. M., 1979. Electrical properties of
559 forsterite, mg_2sio_4 II. *Physical Review B* 19 (6), 2886 – 4445.

560 Morioka, M., 1980. Cation diffusion in olivine - i. cobalt and magnesium.
561 *Geochimica et Cosmochimica Acta* 44, 759 – 763.

562 Nakamura, A., Schmalzried, H., 1983. On the nonstoichiometry and point
563 defects of olivine. *Physics and Chemistry of Minerals* 10 (1), 27 – 37.

564 Nakamura, A., Schmalzried, H., 1984. On the Fe^{2+} - Mg^{2+} interdiffusion in
565 olivine (II). *Berichte der Bunsen Gesellschaft fr Physikalische Chemie* 88,
566 140 – 145.

567 Price, G. D., Parker, S. C., Leslie, M., 1987. The lattice dynamics of forsterite.
568 *Mineralogical Magazine* 51, 157 – 170.

569 Redfern, S. A. T., 1998. Time-temperature-dependent M-site ordering in
570 olivines from high-temperature neutron time-of-flight diffraction. *Physica*
571 *B* 141, 1189–1196.

572 Redfern, S. A. T., Henderson, C. M. B., Wood, B. J., Harrison, R. J., Knight,
573 S. K., 1996. Determination of olivine cooling rates from metal-cation order-
574 ing. *Nature* 381, 407 – 409.

575 Richmond, N. C., Brodholt, J. P., 2000. Incorporation of Fe^{3+} into forsterite
576 and wadsleyite. *American Mineralogist* 85 (9), 1155–1158.

577 Sanders, M. J., Leslie, M., Catlow, C. R. A., 1984. Interatomic potentials for
578 sio_2 . *Journal of the Chemical Society, Chemical Communications*.

579 Smyth, D. M., Stocker, R. L., 1975. Point defect and non-stoichiometry in
580 forsterite. *Physics of the Earth and Planetary Interiors* 10, 183 – 192.

581 Sockel, H. G., Hallwig, D., 1977. Ermittlung kleiner diffusionskoeffizienten
582 mittels SIMS in oxydischen verbindungen. *Mikrochimica Acta Suppl.* 7, 95–
583 107.

584 Sockel, H. G., Hallwig, D., Schachtner, R., 1980. Investigations of slow ex-
585 change processes at metal and oxide surfaces and interfaces using secondary
586 ion mass spectrometry. *Materials science and engineering* 42, 59 – 64.

587 Stocker, R. L., Smyth, D. M., 1977. Effect of enstatite activity and oxygen
588 partial pressure on the point-defect chemistry of olivine. *Physics of the*
589 *Earth and Planetary Interiors* 16, 145–156.

590 Sushko, P. V., Shluger, A. L., Baetzold, R. C., Catlow, C. R. A., 2000a. Em-
591 bedded cluster calculations of metal complex impurity defects: properties of
592 the iron cyanide in NaCl. *Journal of Physics: Condensed Matter* 12, 8257 –
593 8266.

594 Sushko, P. V., Shluger, A. L., Catlow, C. R. A., 2000b. Relative energies of
595 surface and defect states: ab initio calculations for the MgO (001) surface.
596 *Surface Science* 450, 153–170.

597 Tsai, T.-L., Dieckmann, R., 1997. Point defects and transport of matter and
598 charge in olivines, $(\text{Fe}_x\text{Mg}_{1-x})_2\text{SiO}_4$. *Materials Science Forum* 239 - 241,
599 399 – 402.

600 Tsai, T.-L., Dieckmann, R., 2002. Variation of the oxygen content and point
601 defects in olivines, $(\text{Fe}_x\text{Mg}_{1-x})_2\text{SiO}_4$, $0.2 \leq x \leq 1.0$. *Physics and Chemistry*
602 *of Minerals* 29, 680 – 694.

603 Uma, S., Sleight, A. W., 2002. A new bismuth magnesium vanadate with
604 reduced vanadium: $\text{BiMg}_{2.5}\text{V}_{18.5}\text{O}_{38}$. *Journal of Solid State Chemistry* 164,
605 138 – 143.

606 Vočadlo, L., Wall, A., Parker, S. C., Price, G. D. 1995. Absolute ionic diffusion
607 in MgO – computer calculations via lattice dynamics. *Physics of the Earth*
608 *and Planetary Interiors* 88, 193 – 210.

609 Walker, A. M., 2004. Computational studies of point defects and dislocations
610 in forsterite (Mg_2SiO_4) and some implications for the rheology of mantle

611 olivine. PhD, University of London.

612 Walker, A. M., Demouchy, S., Wright, K., 2006. Computer modelling of the
613 energies and vibrational properties of hydroxyl groups in α - and β -Mg₂SiO₄.
614 European Journal of Mineralogy 18, 529 – 543.

615 Walker, A. M., Gale, J. D., Slater, B., Wright, K., 2005. Atomic scale mod-
616 elling of the cores of dislocations in complex materials part 2: applications.
617 Physical Chemistry Chemical Physics 7.

618 Walker, A. M., Wright, K., Slater, B., 2003. A computational study of oxygen
619 diffusion in olivine. Physics and Chemistry of Minerals 30 (9), 536 – 545.

620 Wang, Z. Y., Hiraga, T., Kohlstedt, D. L., 2004. Effect of H⁺ on Fe-Mg in-
621 terdiffusion in olivine, (Fe,Mg)₂SiO₄. Applied Physics Letters 85 (2), 209 –
622 211.

623 Wilson, P., Emmerich, W., Brodholt, J., 2004. Leveraging HTC for UK
624 eScience with very large Condor pools: Demand for transforming untapped
625 power into results. In: Proceedings of the UK e-Science All Hands Meeting
626 2004.

627 Woodley, S. M., Walker, A. M., 2007. New software for finding transition states
628 by probing accessible, or ergodic, regions. Molecular Simulation 33, 1229 –
629 1231.

630 Wright, K., Catlow, C. R. A., 1994. A computer simulation study of (OH)
631 defects in olivine. Physics and Chemistry of Minerals 20, 515 –518.

632 Wright, K., Freer, R., Catlow, C. R. A., 1994. The energetics and structure of
633 the hydrogarnet defect in grossular: a computer simulation study. Physics
634 and Chemistry of Minerals 20, 500 – 503.

Table 1

Defect energies for Mg1 vacancies in forsterite calculated using the embedded cluster method. The basis set code refers to the basis used for geometry optimisation and final energy calculation respectively (so 6-31+G*//6-31G means optimisation using the 6-31G basis with final energy calculation using the 6-31+G* basis). Rapid convergence is observed for each method with basis set size.

Basis set	Defect energy (eV)		
	Hartree-Fock	DFT (PW91)	DFT (B3LYP)
6-31G//6-31G	25.832	27.127	26.875
6-31+G*//6-31G	24.942	25.725	25.564
6-31+G*//6-31+G*	24.979	25.762	25.610
6-311+G*//6-31+G*	25.002	25.780	25.632
6-311+G*//6-311+G*	25.017	25.773	25.625

Table 2

Defect energies for the magnesium split interstitial across the M1 site. The meaning of the basis set symbols are given in the caption to Table 1.

Basis set	Defect energy (eV)		
	Hartree- Fock	DFT (PW91)	DFT (B3LYP)
6-31G//6-31G	-18.029	-18.470	-18.478
6-31+G*//6-31G	-17.366	-17.952	-17.947
6-31+G*//6-31+G*	-17.403	-18.001	-17.993
6-311+G*//6-31+G*	-17.503	-18.045	-18.038
6-311+G*//6-311+G*	-17.508	-18.049	-18.043

Table 3

Migration energies for magnesium vacancy and interstitial diffusion in forsterite.

Hop	Defect energy of initial state (eV)	Defect energy of activated state (eV)	Migration energy (eV)
A	24.48	30.37	5.89
B	26.40	35.50(a)	9.10
C	26.40	27.87(a)	1.47
D	24.48	26.46	1.98
D'	26.40		0.06
E	24.48	30.94(a)	4.54
E'	26.40		6.64
F	24.40	25.12	0.72
Interstitial // [100]	-17.75	-13.86	3.89
Interstitial // [010]	-17.75	-13.86	3.89
Interstitial // [001]	-17.75	-14.62	3.13

(a) These failed to converge in the RFO part of the calculation and so an estimate of the transition state is made from the initial search, where the moving ion is fixed and the rest of the structure relaxed, is used, the true energy of the activated state is not expected to be significantly different from this estimate.

Table 4

Defect energies for a range of possible intrinsic defects in forsterite

Defect ^a	Mott-Littleton method (eV)
$V_{O1}^{\bullet\bullet}$	27.97 ^b
$V_{O2}^{\bullet\bullet}$	25.20
$V_{O3}^{\bullet\bullet}$	24.54
$O''_{I(1)}$	-14.37
$O''_{I(2)}$	-16.11
V''_{Mg1}	24.48
V''_{Mg2}	26.40
$Mg^{\bullet\bullet}_{I(split)}$	-17.75
V''''_{Si}	100.81 ^c
$Si_I^{\bullet\bullet\bullet\bullet}$	-76.60
Fe^{\bullet}_{M1}	-22.55 ^d
Fe^{\bullet}_{M2}	-23.24
$U(Mg_2SiO_4)$	-212.49
$U(MgSiO_3)$	-171.97
$U(Fe_2O_3)$	-150.37
$U(MgO)$	-41.31

^a Defects are described using Kröger-Vink defect notation and include vacancies in all three oxygen positions, oxygen interstitial ions occupying both free octahedral sites on both magnesium sites, a split interstitial magnesium defect, a silicon vacancy and a silicon interstitial. Defect energies are quoted with respect to the perfect forsterite lattice and the ion at infinity.

^b Energies of oxygen defects are from Walker et al. (2003)

^c Energies of silicon defects are from Walker (2004)

^d Energies of iron defects are from Walker et al. (2003)

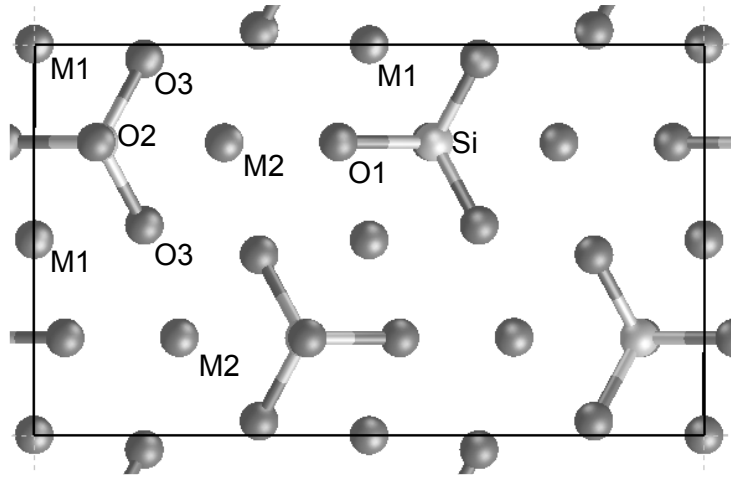


Fig. 1. Unit cell of the olivine structure viewed along $[100]$. The long visible cell axis is $[010]$ and the shorter one is $[001]$, occupied sites are marked.

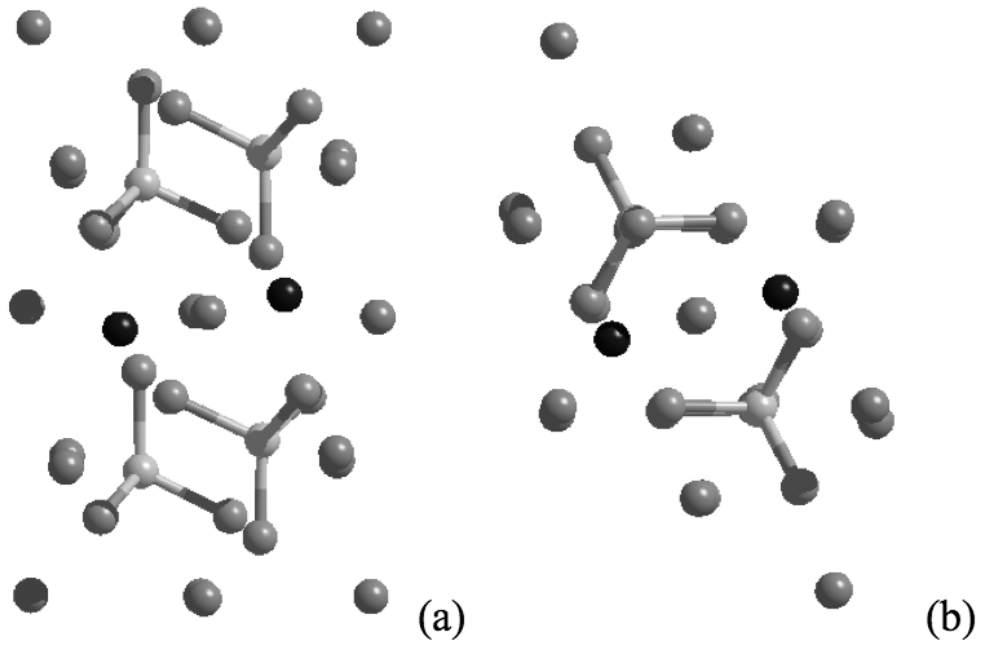


Fig. 2. Structure of magnesium split interstitial defect from embedded cluster calculations. (a) Looking along $[010]$ with $[100]$ oriented up the page. (b) Looking along $[100]$ with $[001]$ oriented up the page. The two tetrahedral magnesium ions are shown in black, otherwise magnesium ions isolated spheres, silicon and oxygen ions form SiO_4 tetrahedra.

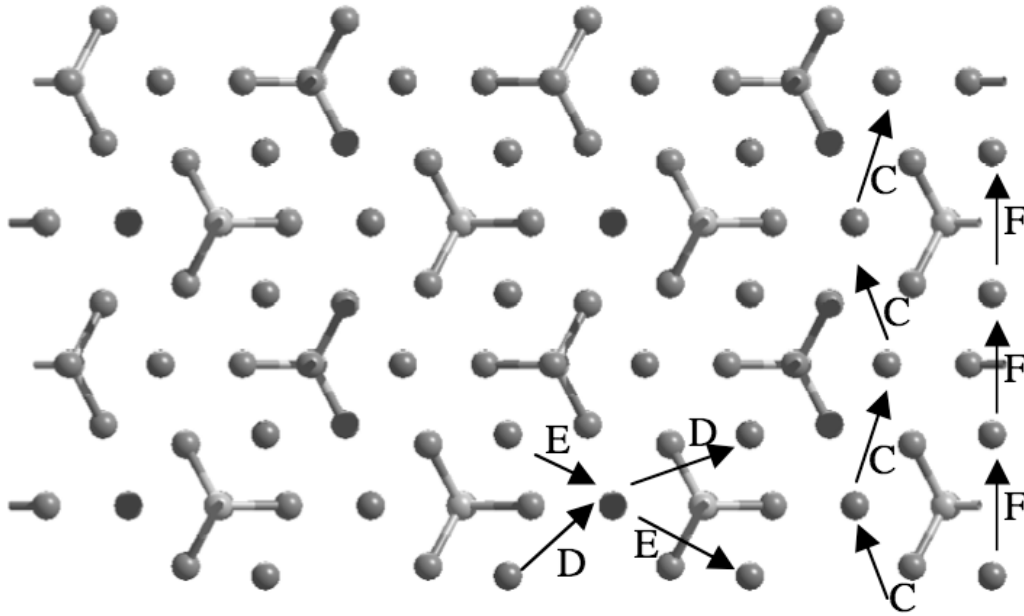


Fig. 3. Magnesium diffusion by the vacancy mechanism (see text for details) projected onto the (100) plane. Hops A and B are not shown as they are perpendicular to the plane.